Structural refinement of superlattices from x-ray diffraction

Eric E. Fullerton and Ivan K. Schuller
Physics Department 0319, University of California-San Diego, La Jolla, California 92093

H. Vanderstraeten and Y. Bruynseraede
Laboratorium voor Vaste Stof-Fysika en Magnetisme, Katholieke Universiteit Leuven, B-3001 Leuven, Belgium
(Received 17 May 1991)

We present a general procedure for quantitative structural refinement of superlattice structures. To analyze a wide range of superlattices, we derived a general kinematical diffraction formula that includes random, continuous, and discrete fluctuations from the average structure. We show that only the structure factor of one single layer of each material has to be averaged over the random variables and prove that this relation is equivalent to earlier, less general models. Implementing a nonlinear-fitting algorithm to fit the entire x-ray-diffraction profile, refined parameters that describe the average superlattice structure and deviations from this average are obtained. We compare the results of structural refinement to results obtained independently from other measurements. The roughness introduced artificially during growth in Mo/Ni and Nb/Cu superlattices is accurately reproduced by the refinement. The lattice parameters of Ag/Mn obtained from this refinement procedure are in very good agreement with the values obtained from independent extended x-ray-absorption fine-structure and x-ray photoelectron diffraction studies. The relative thicknesses of the layers can be accurately determined, as proved for Cu/Ni in comparison with chemical analysis, for W/Ni compared to the calibrated sputtering rate, and for Mo/Ni compared to the low-angle profile.

I. INTRODUCTION

The study of superlattice structures has received increased interest in recent years as a result of the wide range of new physical phenomena observed in these systems. The presence of the additional periodicity of the layered material often leads to unique magnetic, transport, mechanical and superconducting properties.[1] By changing the material in each layer and the layer thicknesses, it is often possible to optimize the desired properties of the system. Many applications for superlattices are being pursued, including mirrors for soft x rays[2] and neutrons,[3] high-critical-current superconductors,[4] magnetoresistive heads,[5] and magneto-optical recording materials.[6] Superlattices are also useful systems for studying thin-film, interface, and coupling effects, because a large volume sample can be prepared and surface contamination can thus be avoided.

Understanding the physical properties is limited by the characterization of the samples. Many of the physical properties depend sensitively on structural properties such as interdiffusion, crystallinity, strain, and roughness, making structural characterization a prerequisite to understanding the physical properties. Superlattices are usually made by deposition techniques such as sputtering or evaporation, and are not in thermodynamic equilibrium. Therefore, the structure is strongly dependent on growth conditions.

X-ray diffraction is a technique that is well suited for studying the structure of superlattices. It is nondestructive and can provide structural information on the atomic scale. Because the scattered x-ray intensity is measured, the phase information is lost and it is impossible to directly convert the intensities to obtain the structure. Modeling of the superlattice is required to compare the calculated intensity of the modeled superlattice with the measured intensity. By fitting the measured intensity profiles with model calculations, it is possible to obtain the structure. This type of structural characterization is commonly used in x-ray and neutron diffraction from bulk powder crystals using the Rietveld refinement procedure.[7,8] In Rietveld refinement, the structure of a single unit cell is modeled. The relative intensity of the diffraction peaks is determined from the structure factor of the unit cell and the line profiles are fit to a structurally independent profile shape function. The difference with the present refinement technique is that the relative intensities *and* line profiles are used to determine the average unit cell *and* the deviations from this average.

The characteristic length scales in superlattices are (i) the modulation wavelength Λ defined as the repeat distance of the layering, (ii) the lattice spacing of the constituent material, and (iii) the structural coherence length ξ, which is the distance over which the atomic positions are quantitatively correlated and can be estimated from the full width at half maximum of diffraction peaks using Scherrer's equation.[9] In many superlattices, ξ is limited to only a few times Λ due to structural disorder. The type and amount of structural disorder can greatly affect the relative intensity of the diffraction peaks. Since many types of disorder can be present in a superlattice, including layer thickness fluctuations, interface disorder, crystalline disorder, and interdiffusion, a large number of model parameters have to be included. This makes a refinement procedure much more difficult.

In this paper we present a general kinematic diffraction

model that includes both the average atomic structure of the layers and structural disorder for fitting measured x-ray-diffraction profiles. By fitting the measured profiles, it is possible to *quantitatively* determine both lattice constants and disorder parameters of a wide variety of superlattices. To illustrate the need to include lattice deviations and structural disorder in superlattice calculations, Fig. 1 shows the measured x-ray-diffraction profile (open circles) of a sputtered Mo/Ni superlattice compared to two model calculations. The thin line is calculated assuming a perfect superlattice with bulk lattice parameters for the Mo and Ni. The thick line is the result of the refinement procedure described in this paper which quantitatively fits the measured diffraction profile over 3 orders of magnitude in intensity.

First, we will review previous modeling of disordered superlattices and describe the theoretical formalism we have developed, which combines the various disorder parameters into one single model. This formalism allows direct fitting of the full x-ray-diffraction profiles, including line shapes and relative intensities as shown in Fig. 1, and has been applied to diffraction profiles from metallic superlattices made by sputtering, evaporation, and electroplating. To determine the reliability of structural parameters determined from the refinement procedure, we have studied a large number of samples in which structural parameters can be determined independently. In all cases, good, quantitative agreement is obtained.

II. EARLIER WORK

The θ-2θ x-ray-diffraction profile is commonly divided into two regions, low angle ($\lesssim 15°$) and high angle ($\gtrsim 15°$).[1] The low-angle region is a result of scattering from the chemical modulation of the layers. The position of the peaks is given by[10]

$$\sin^2\theta = \left[\frac{n\lambda_x}{2\Lambda}\right]^2 + 2\bar{\delta}_s \ , \tag{1}$$

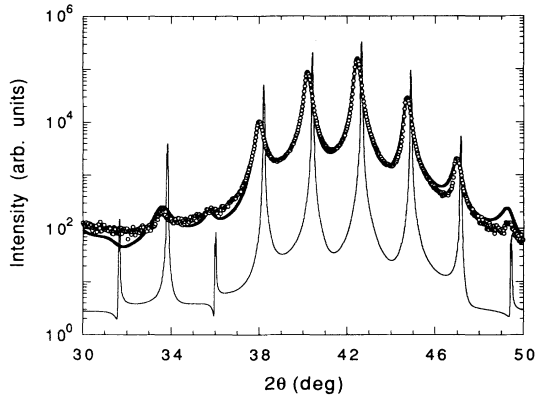

FIG. 1. Measured x-ray-diffraction profile of a [Mo(20 Å)/Ni(22 Å)]$_{130}$ superlattice (circles) and calculated spectra (thin line) using formalism described in Ref. 13 assuming bulk Mo and Ni lattice spacing and integer number of atomic layers. Thick line is the result of refinement procedure described in text.

where θ is angle of the peak position, n the order of reflection, λ_x is the x-ray wavelength, and $1-\bar{\delta}_s$ is the real part of the average index of refraction of the superlattice. The value of $\bar{\delta}_s$ is typically $\approx 3\times 10^{-5}$, which only leads to significant deviations from Bragg's law for 2θ values less than 3° for Cu radiation. The high-angle portion of the profiles depends strongly on the structural coherence length normal to the layers. If $\xi < \Lambda$, then the peak positions correspond to the lattice spacings of the constituent materials. This often occurs when the layers are very thick, when one of the materials is amorphous,[11] or in superlattices with large lattice mismatch.[12] If $\xi > \Lambda$, then superlattice peaks are observed with positions determined by Eq. (1). For convenience, the high-angle peak positions are usually indexed about the average lattice constant $\bar{d}$:

$$2\frac{\sin\theta}{\lambda_x} = \frac{1}{\bar{d}} \pm \frac{n}{\Lambda} \ , \tag{2}$$

where n is an integer that labels the order of the satellite around the main Bragg peak and $\bar{d} = \Lambda/(N_A + N_B)$, where N_A and N_B are the number of atomic planes of material A and B in one bilayer. The only quantities that can be determined directly from the peak positions are $\bar{d}$ and Λ and an estimate for ξ may be obtained from the linewidth. The individual lattice parameters of the constituent materials and the disorder and consequent mechanism determining ξ requires modeling of the superlattice.

A. High-angle intensity calculations

A variety of superlattice models have been based on one-dimensional step-model calculations.[13] The peak positions are determined by Eq. (2) and the relative intensities are given by the square of the scattering factor of a single bilayer. The step-model calculations assumed an abrupt composition profile with bulk lattice spacings for each material. The models were able to *qualitatively* reproduce the measured x-ray-diffraction profiles of Nb/Cu superlattices. The step model has been refined to include lattice spacing variations due to in-plane coherency strain, atomic interdiffusion, and compound formation at the interface.

Strain models are commonly used to determine the structure of semiconductor superlattices.[14,15] The simplest strain model assumes an integer number of molecular layers with a uniform lattice spacing throughout the layer. The relative intensities of the superlattice peaks are fit by adjusting the number of molecular layers and lattice spacing of each layer. The strain is then determined from the fit values of the lattice spacing. More detailed models have included strained interfacial layers[16] or chemically mixed interfacial layers.[17]

In samples in which a chemical and/or strain profile is assumed, the scattering power and the lattice spacing can be approximated by Fourier series expansions.[18,19] If the expansion is limited to the second term, then the amplitude of the first- and second-order superlattice peaks can be calculated. Such a model has been used to estimate the compositional profile in superlattices.[20,21] In many

cases, a specific functional form (e.g., linear[22] or an error function[23]) for the compositional profile is assumed where the lattice spacings in the interface are assumed to be proportional to the composition in the plane according to Vegard's law. The main fitting parameter of the model is the width of the interdiffusion region. Such models have been successful in understanding the evolution of diffraction profiles of superlattices during ion irradiation.[24] The interdiffusion region can also be replaced in calculations by a compound of the constituent material.[25]

B. Low-angle intensity calculations

In principle, the low-angle diffraction profile gives directly the Fourier transform of the compositional profile, but disorder, multiple reflections (dynamical corrections), refraction effects, and surface reflections limits the information obtainable from a Fourier transform of the diffraction profile. The most common approach to calculate the low-angle profile is the recursive application of optical theories[26,27] where the layers are assumed to be a continuous medium and the reflection at each interface is calculated. These theories have been shown to be equivalent to dynamical calculations[28] and include effects of absorption, refraction, and surface and substrate reflections. The effects of interdiffusion can be directly included in these models.[26]

C. High-angle disorder calculations

The fitting of the composition and strain profile is a measure of the structure of the average bilayers in the growth direction, but does not address the problem of the type and magnitude of structural fluctuations in the superlattice. In superlattice structures there are many types of random fluctuations that are cumulative,[11] leading to a loss of long-range order. There are several mechanisms that can cause disorder, including variations in deposition rates and growth modes, misfit dislocations, and interface disorder from incommensurate lattice mismatched interfaces. Because it is generally impossible to deposit exactly an integer number of atomic planes in each layer, there will be a minimum of one atomic plane fluctuation in the layers.[29,30] The original intensity calculations which included the effects of random sequencing of layers were done by Hendricks and Teller[31] and were later formulated for a finite number of layers.[32–34] The result of these calculations was broadened diffraction lines and an increased amount of diffuse scattering with increasing disorder.

More recently, a number of models based on the Hendricks-Teller approach have been proposed. These include random cumulative fluctuations in the modulation wavelength, layer thicknesses, and interface distances. In most cases, the fluctuations are assumed to be Gaussian distributed. The amount of broadening is strongly dependent on whether the distribution is continuous or discrete. Sevenhans *et al.*[11] demonstrated that 1.4 Å of continuous layer thickness fluctuations of the amorphous layer in a crystalline-amorphous superlattice results in the loss of all high-angle superlattice peaks and the high-angle profile becomes representative for a single crystalline layer. This paper also showed that the total scattering intensity $I(q)$ (diffuse and Bragg) requires the calculation of $\langle F_{SL}(q)F^*_{SL}(q)\rangle$ and not $\langle F_{SL}(q)\rangle\langle F^*_{SL}(q)\rangle$, where $F_{SL}(q)$ is the scattering amplitude of the superlattice and brackets indicate the average over the random continuous fluctuations. Many model calculations averaged the scattering amplitude[20,35] giving only the Bragg component of scattering intensity. Clemens and Gay[36] showed that, if layer thickness fluctuations of a crystalline layer are discrete through a variable integer number of atomic layers, then a much smaller broadening of the superlattice diffraction peaks is observed.

Model calculations for crystalline-crystalline superlattices which assumed continuous fluctuations of the interface width between materials A and B (Ref. 37) explained the loss of long-range order in a number of lattice-mismatched superlattices. It was found that the derived amount of interface disorder was of the order of the difference of the lattice spacing of the constituent materials. Although this model could explain several features of the high-angle profiles, realistic values for the roughness could not explain the limited number of low-angle peaks observed in many superlattices. The model was therefore extended to include discrete disorder in each of the layers.[38] By including discrete fluctuations in the layers and continuous fluctuations at the interface, both low- and high-angle profiles in some metallic superlattices could be understood. These calculations showed that the amount of broadening of the high-angle superlattice peaks is strongly dependent on the difference of the lattice spacing. Lattice-matched superlattices are less sensitive to discrete disorder than lattice mismatched systems. The model also showed that a larger discrete disorder in one of the layers tends to broaden the superlattice peaks corresponding to the other material.

D. Low-angle disorder calculations

The effect of disorder on low-angle profiles has been extensively studied, particularly related to the application of superlattices as x-ray mirrors.[2,27,39–41] In low-angle calculations, roughness is commonly simulated by multiplying the calculated intensity by an effective Debye-Waller coefficient,[2,26] or treating a rough interface as an alloy region.[42] This kind of formalism only treats lateral noncumulative roughness and does not affect the peak widths. Calculations that include random layer thickness fluctuations[2,12,38,43–45] have, in general, found (i) increased layer thickness fluctuations decreases intensity *and* increases line widths, (ii) the higher-order peaks are more strongly affected by the layer thickness fluctuations, and (iii) the intensity between peaks increases and the finite-size peak intensities decrease with increased layer thickness fluctuations.

III. THEORETICAL FORMALISM

A. High-angle kinematic formalism

To fit the measured x-ray-diffraction profiles with a wide range of different models, we have developed a gen-

eral kinematical expression which includes both discrete and continuous cumulative disorder. Discrete thickness disorder assumes that the thickness is varying by an integer number of atomic planes. Continuous disorder refers to structural parameters that vary in a continuous way like the thickness of an amorphous layer. The types of disorder that will be discussed can be separated into intralayer and interlayer disorder. Intralayer disorder refers to the quality of the atomic ordering within a single layer. A crystalline layer has a high degree of intralayer order, while an amorphous layer is not ordered. Interlayer disorder refers to the deviation in the periodicity of the layers in the growth direction resulting from layer thickness variations and interface disorder.

The general model of a superlattice consists of a stack of M bilayers of material A and B, shown in Fig. 2. The layers are characterized by the structure factors F_{Aj}, F_{Bj}, and thicknesses t_{Aj}, t_{Bj} of materials A, B in the jth bilayer and the interface distances separating the layers are given by a_{Aj} and a_{Bj}. The model in Fig. 2 explicitly includes only interlayer disorder and makes no assumptions about the crystal structure of the layers which are considered unit scatterers described by F_{Aj} and F_{Bj}. The one-dimensional structure factor for a superlattice with M bilayers with cumulative layer thickness fluctuations can be written as

$$F_{\mathrm{SL}}(q)=\sum_{j=1}^{M}\exp(iqx_j)\{F_{Aj}+\exp[iq(t_{Aj}+a_{Aj})]F_{Bj}\}\ , \tag{3}$$

where

$$x_j=\sum_{s=1}^{j-1}t_{As}+a_{As}+t_{Bs}+a_{Bs}\ ,$$

and q is the scattering vector given by $q=4\pi\sin\theta/\lambda_x$. The scattering intensity is given by $I(q)=\langle F_{\mathrm{SL}}(q)F^{*}_{\mathrm{SL}}(q)\rangle$, where the brackets are an ensemble average over all possible F_{Aj}, F_{Bj}, t_{Aj}, t_{Bj}, a_{Aj}, and a_{Bj}. The expression for $I(q)$ can be written in closed form if each layer is assumed to be statistically independent, similar to the original Hendricks-Teller approach.

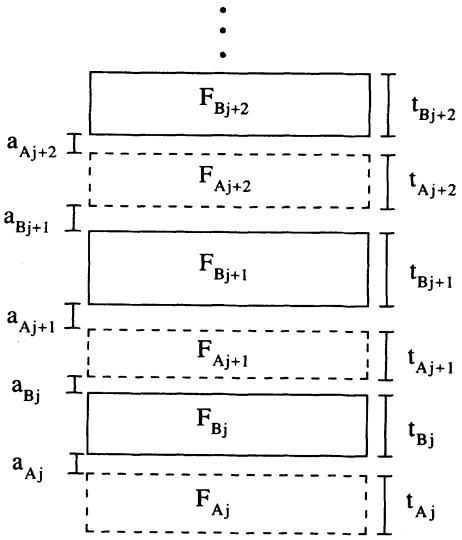

FIG. 2. Representation of a superlattice consisting of layers of materials A and B, with thicknesses $t_{A,j}$, $t_{B,j}$ and structure factors $F_{A,j}$, $F_{B,j}$. The layers are separated by interface distances $a_{A,j}$ and $a_{B,j}$.

For a lattice-mismatched incoherent interface, the lattice positions are not well defined, which leads to variations in the interface distance. Therefore, we will assume that the interface distances a_{Aj} and a_{Bj} vary in a continuous manner, as was done in our previous work.[37,38] To simulate such variations, a Gaussian distribution about an average value a_A is assumed:

$$P(a_{Aj})=\frac{1}{\sqrt{2\pi}c}\exp\left[-\frac{(a_{Aj}-a_A)^2}{2c^2}\right]\ , \tag{4}$$

where c is the interface fluctuation width. An identical expression is used for $P(a_{Bj})$, where a_A and a_B are assumed to be equal and will be given as a. The interface distances are averaged by integrating $P(a_{Aj})F(q)F^{*}(q)$ over all interface distance values. With these assumptions, the intensity for a superlattice with M bilayers can be written as[46]

$$\begin{aligned}I(q)=M\{&\langle F_AF_A^{*}\rangle+2\,\mathrm{Re}[e^{\zeta}\Phi_A\bar{F}_B]+\langle F_BF_B^{*}\rangle\}\\&+2\sum_{r=1}^{M-1}(M-r)\mathrm{Re}[e^{2r\zeta}(\Phi_A\bar{F}_AT_A^{r-1}T_B^{r}+\Phi_B\bar{F}_BT_A^{r}T_B^{r-1})\\&+e^{(2r-1)\zeta}\Phi_B\bar{F}_AT_A^{r-1}T_B^{r-1}+e^{(2r+1)\zeta}\Phi_A\bar{F}_BT_A^{r}T_B^{r}]\ ,\end{aligned} \tag{5}$$

where $\zeta=iqa-q^2c^2/2$, Re designates the real part of the term in the bracket and the following averaged parameters are defined by

$$\begin{aligned}&\bar{F}_A=\langle F_A\rangle,\quad \bar{F}_B=\langle F_B\rangle\\&\Phi_A=\langle\exp(iqt_A)F_A^{*}\rangle,\quad \Phi_B=\langle\exp(iqt_B)F_B^{*}\rangle\\&T_A=\langle\exp(iqt_A)\rangle,\quad T_B=\langle\exp(iqt_B)\rangle\ .\end{aligned} \tag{6}$$

Because the layers are assumed to be statistically independent, the expression for $I(q)$ can be written in terms of the averaged parameters of the layers of material A and B [Eq. (6)] independent of the number of layers in the superlattice. The first term in Eq. (5) is the scattering from M individual bilayers. The terms within the sum are from the interference between bilayers which are offset by r bilayers with respect to each other. After averaging, there are $M-r$

equivalent pairs of bilayers offset by r bilayers. By separating the terms depending on r, Eq. (5) can be written in closed form as

$$I(q)=M[\langle F_A F_A^* \rangle + 2\,\mathrm{Re}(e^{\xi}\Phi_A \bar{F}_B)+\langle F_B F_B^* \rangle]+2\,\mathrm{Re}\left[(e^{-\xi}\Phi_B \bar{F}_A T_A^{-1} T_B^{-1}+\Phi_A \bar{F}_A T_A^{-1}+\Phi_B \bar{F}_B T_B^{-1}+e^{\xi}\Phi_A \bar{F}_B) \times \left[\frac{M-(M+1)e^{2\xi}T_A T_B+(e^{2\xi}T_A T_B)^{M+1}}{(1-e^{2\xi}T_A T_B)^2}-M\right]\right] . \tag{7}$$

To calculate $I(q)$ for an explicit model using Eq. (7), the averaged quantities Φ_A, Φ_B, T_A, T_B, $\bar{F}_A$, $\bar{F}_B$, $\langle F_A F_A^* \rangle$, and $\langle F_B F_B^* \rangle$ have to be calculated. These averaged quantities include both the average structure of the layers and the statistical fluctuations of the layers throughout the stack. For discrete disorder, the averages can be calculated by summing over all the possible F_{Aj} and F_{Bj} with corresponding t_{Aj} and t_{Bj} weighted by the probability of occurrence. Continuous disorder requires integration of the bracketed quantity over all possible values of the continuous variable, weighted by the probability of occurrence. The effect of these fluctuations on the x-ray-diffraction profile of a superlattice is determined by the parameters of a single unit cell. The power of Eq. (7) is that *the averages needed are only over a single layer and not the superlattice,* which greatly facilitates the calculation of a wide range of models. Superlattices with very complicated structures, such as high-temperature superconductor superlattices, can be directly simulated once the scattering factors of the individual layers can be calculated. Equation (7) can be further reformulated to approximate any layered structure (e.g., more than two layers in the superlattice unit cell). If the disorder is random, then $I(q)$ for that model can be written in terms of the average scattering power of the individual layers.

We will now give examples of Φ_A, Φ_B, T_A, T_B, $\bar{F}_A$, $\bar{F}_B$, $\langle F_A F_A^* \rangle$, and $\langle F_B F_B^* \rangle$ for some specific models. The specific type of structural order within a layer can be crystalline, amorphous, or any other suitably chosen structure. In most previous model calculations of structural disorder, an analytical relation for the intensity was derived for perfectly crystalline or amorphous layers and a specific type of structural disorder. Other calculations that combined a nonideal atomic structure for the layers and structural disorder averaged the intensity numerically.[47] We will first discuss structures that were used in earlier model calculations and then extend the discussion to more complicated structures.

If we take the layers in a crystalline-crystalline superlattice as perfect crystals in which there is an integer number of atomic layers separated by a constant lattice spacing, F_A and F_B are given by

$$F_{Aj}=f_A\frac{1-\exp(iqN_{Aj}d_A)}{1-\exp(iqd_A)} ,$$
$$F_{Bj}=f_B\frac{1-\exp(iqN_{Bj}d_B)}{1-\exp(iqd_B)} , \tag{8}$$

where N_A (N_B), f_A (f_B) and d_A (d_B) are, respectively, the number of atomic layers, the scattering power of an atomic plane, and the crystalline lattice spacing of material A (B). The layer thicknesses are given simply by $t_{Aj}=(N_{Aj}-1)d_A$ and $t_{Bj}=(N_{Bj}-1)d_B$. Assuming there is no variation in N_A or N_B [so no averages are required for the terms in Eq. (6)] and considering only the continuous fluctuations at the interface, Eq. (7) is equivalent to Eq. (1) in Ref. 37. It was shown there that continuous interface fluctuations broaden all the superlattice peaks.

The effects of discrete layer thickness fluctuations can be included by assuming a discrete Gaussian variation of N_{Aj} and N_{Bj} about an integer average value N_A and N_B. The Gaussian distribution assumed is given by[38]

$$P(N_{Aj})=\frac{1}{K}\exp\left[\frac{(N_{Aj}-N_A)^2}{-2\omega_A^2}\right] ,$$
$$K=\sum_{j=0}^{\infty}P(N_{Aj}) , \tag{9}$$

where ω_A is the width of the discrete fluctuations and K is the normalization constant. A similar expression is assumed for $P(N_{Bj})$. The averaged terms in Eqs. (6) and (7) for layer A are given by

$$\bar{F}_A=\sum_{j=0}^{\infty}P(N_{Aj})F_{Aj} ,$$
$$\Phi_A=\sum_{j=0}^{\infty}P(N_{Aj})\exp[(N_{Aj}-1)iqd_A]F_{Aj}^* ,$$
$$T_A=\sum_{j=0}^{\infty}P(N_{Aj})\exp[(N_{Aj}-1)iqd_A] , \tag{10}$$
$$\langle F_A F_A^* \rangle=\sum_{j=0}^{\infty}P(N_{Aj})F_{Aj}F_{Aj}^* .$$

There are equivalent terms for layer B. When the terms in Eq. (10) are used in Eq. (7), the resulting expression is equivalent to Eq. (4) in Ref. 38 and the results for discrete disorder in Ref. 36. In practice, the sums in Eq. (10) can be limited to $\pm 3\omega_A$ of N_A and can be calculated numerically.

The effects of an amorphous material in a crystalline-amorphous or amorphous-amorphous superlattice can be calculated by assuming the amorphous layer to be a layer of constant scattering density. The scattering factor of a single amorphous layer can be written as

$$F_j=\int_0^{t_j}\rho\exp(iqz)dz=\frac{\rho}{iq}[\exp(iqt_j)-1]\ , \tag{11}$$

where ρ is the scattering power per unit volume, which for low angles is approximately the electron density, and t_j is the layer thickness. Assuming that the layer thicknesses t_j vary in a continuous Gaussian distribution with width, σ around an average thickness t, the averaged terms can be determined by integrating over all real values of t_j.[46]

$$\begin{aligned}
&\bar{F}=\frac{i\rho}{q}[1-\exp(iqt-q^2\sigma^2/2)]\ ,\\
&\Phi=\frac{i\rho^*}{q}[1-\exp(iqt-q^2\sigma^2/2)]\ ,\\
&T=\exp(iqt-q^2\sigma^2/2)\ ,\\
&\langle FF^*\rangle=\frac{2\rho\rho^*}{q^2}[1-\exp(-q^2\sigma^2/2)\cos(qt)]\ .
\end{aligned} \tag{12}$$

By combining Eq. (12) with the crystalline model given by Eq. (10), the diffraction profiles of crystalline-amorphous superlattices can be simulated. As was shown earlier by Sevenhans *et al.*,[11] a continuous layer thickness disorder of $\sigma\approx 1.4$ Å destroys any indication of superlattice structure in the high-angle region. In this region, Eq. (12) is very similar to the crystalline-crystalline equation where the amorphous layer is simulated by setting its scattering power to zero. For kinematic low-angle calculations of an amorphous-crystalline superlattice, setting the scattering power to zero is not a valid assumption because the low-angle diffraction spectra is not as sensitive to the crystal structure but measures the contrast in electron density of the layers. Therefore, Eq. (12) is needed.

To simulate an intralayer disorder, intermediate between that given by Eqs. (8) and (11), the positions of the atomic planes of a crystalline layer are allowed to vary randomly. If this process is noncumulative, the effect of the variation will be equivalent to thermal variations and can be modeled as an effective Debye-Waller parameter multiplied to the scattering factor with the atomic layer. If the disorder is cumulative, the scattering factor of a layer with N atomic planes is given by

$$F=f\sum_{j=0}^{N-1}\exp\left[iq\left[jd+\sum_{r=1}^{j}\partial_r\right]\right]\ , \tag{13}$$

where f is the atomic scattering power of an atomic plane, d is the atomic plane spacing, and ∂_j is the deviation of the $(j+1)$th atomic plane. If the values ∂_j are assumed to vary independently in a continuous Gaussian distribution about zero with a width δ, the averaged terms in Eq. (6) for a given integer value of N can be written as

$$\begin{aligned}
&\bar{F}=f\left[\frac{1-e^{N\beta}}{1-e^{\beta}}\right]\ ,\\
&\Phi=f^*\left[\frac{1-e^{N\beta}}{1-e^{\beta}}\right]\ ,\\
&T=e^{(N-1)\beta}\ ,\\
&\langle FF^*\rangle=ff^*\left[-N+2\,\mathrm{Re}\left[\frac{N-(N+1)e^{\beta}+e^{(N+1)\beta}}{(1-e^{\beta})^2}\right]\right]\ ,
\end{aligned} \tag{14}$$

where $\beta=iqd-q^2\delta^2/2$. To include discrete disorder in the number of layers, the averaged quantities in Eq. (14) must be summed for all possible values of N weighted by the probability of occurrence analogous to Eq. (10). Figure 3 shows the calculated profiles for a Mo(40 Å)/Ni(40 Å) superlattice with increasing intralayer disorder δ_{Ni} in the Ni layer. For $\delta_{\mathrm{Ni}}=0$, Eq. (14) reduces to the perfect crystalline layer given by Eq. (10). For increasing δ_{Ni}, all the superlattice peaks broaden due to the increased continuous disorder [in a similar way as the interface parameter c in Eq. (7)] and the intensity of the Ni diffraction peaks decrease. For large δ_{Ni}, the Ni layer is essentially amorphous with large continuous layer thickness fluctuations that destroys any indication of superlattice structure. Only the Mo diffraction peak with finite-size fringes survives.

Equation (7) can be extended to a two-dimensional structure. It has been shown that, to account for the observed low-angle profiles in Pb/Cu superlattices,[12] an additional in-plane averaging of the scattering amplitude is required. Observed dips in these profiles could be reproduced by a finite averaging including the phase information before the intensity averaging is done. Equation (3) can be extended to include in-plane averaging for the two-dimensional model shown in Fig. 4. The structure factor of L columns with M bilayers is averaged where each column is assumed to be statistically independent. The structure factor is given by

$$F_{\mathrm{SL}}(q)=\sum_{k=1}^{L}\sum_{j=1}^{M}\exp(iqx_{j,k})\{F_{Aj,k}+\exp[iq(t_{Aj,k}+a_{Aj,k})]F_{Bj,k}\}\ , \tag{15}$$

where

$$x_{j,k}=t_{S,k}+\sum_{s=1}^{j-1}(t_{As,k}+a_{As,k}+t_{Bs,k}+a_{Bs,k})\ ,$$

and $t_{S,k}$ is the deviation of the substrate from its average value for the kth column. The intensity scattered by the superlattice can be written

$$I(q)=LI_S(q)+(L-1)L\langle\exp(iqt_S)\rangle\langle\exp(-iqt_S)\rangle$$
$$\times\sum_{j=1}^{M}\sum_{k=1}^{M}\mathrm{Re}(\exp[2(j-k)iqa-2(j+k-2)q^2c^2/2]\bar{F}_A\bar{F}_A^*T_A^{j-1}T_B^{j-1}T_A^{*k-1}T_B^{*k-1}$$
$$+\exp\{[2(j-k)+1]iqa-[2(j+k)-3]q^2c^2/2\}\bar{F}_B\bar{F}_A^*T_A^jT_B^{j-1}T_A^{*k-1}T_B^{*k-1}$$
$$+\exp\{[2(j-k)-1]iqa-[2(j+k)-3]q^2c^2/2\}\bar{F}_A\bar{F}_B^*T_A^{j-1}T_B^{j-1}T_A^{*k}T_B^{*k-1}$$
$$+\exp[2(j-k)iqa-2(j+k-1)q^2c^2/2]\bar{F}_B\bar{F}_B^*T_A^jT_B^{j-1}T_A^{*k}T_B^{*k-1}). \quad (16)$$

$I_S(q)$ is the intensity from a single column given by Eq. (7) and q is again assumed to be perpendicular to the surface. As before, this equation is independent of the assumptions of the crystal structure of the layers and requires only the ensemble average of a single layer. The inclusion of in-plane averaging has a relatively small effect on the high-angle calculations, but can have a much larger effect on the low-angle calculations. In particular, the line shapes of low-angle peaks can be dramatically changed by the inclusion of in-plane averaging resulting from interference from the columns.

B. Low-angle dynamical formalism

The short coherence length observed in the high-angle diffraction profiles of most metallic superlattices makes the use of a kinematic formalism a very good approximation. In the low-angle region where the length scales probed are of the order of Λ, the coherence length can be much longer and the kinematic assumption is no longer as good. A formalism including dynamical corrections and absorption is needed. Additional corrections at very low angles ($2\theta \lesssim 3°$) are needed for total external reflection from the surface and shift of the peak position due to refraction. To calculate the low-angle profiles we use a standard optical theory by applying a recursive Fresnel formalism described by Underwood and Barbee[26] to the structural models shown in Figs. 2 and 4. This has been shown to be equivalent to dynamical calculations[28] and automatically includes the other low-angle corrections. An equivalent calculation can be accomplished by a matrix formalism where each layer and interface is characterized by a matrix and the superlattice by the product of the matrices.[48] We have not been able to obtain a closed form expression in terms of the ensemble average of a single layer. In previous calculations that include averaging of the layer fluctuations, the reflectivity including the phase information was averaged ($I=|\langle R\rangle|^2$) and not the intensity ($I=\langle|R|^2\rangle$).[45]

To accomplish averaging of the intensity in the absence of an analytical expression, we ensemble average numerically. The formalism described by Underwood and Barbee[26] determines the performance of a superlattice by the recursive use of the single-film Fresnel coefficients. The layers are treated as continuous media with constant electron densities. The formalism determines the reflectance at the interface and propagation through the layers of a plane wave. The recursion procedure starts at the substrate. The reflected wave from the substrate is propagated up through the initial layer of the superlattice to the first interface and added to the reflected wave from that

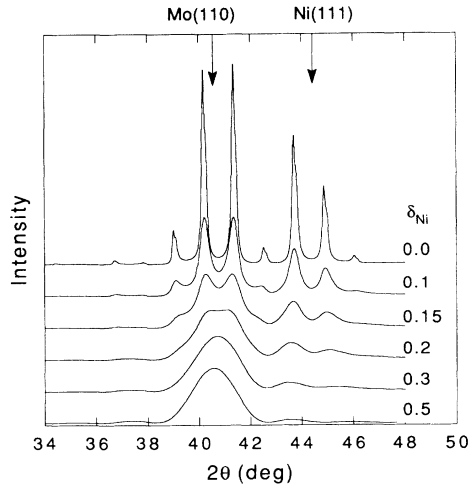

FIG. 3. Simulated x-ray-diffraction profile of a Mo(40 Å)/Ni(40 Å) superlattice without random intralayer disorder in Mo ($\delta_{Mo}=0$), and increments of the disorder δ_{Ni} in Ni.

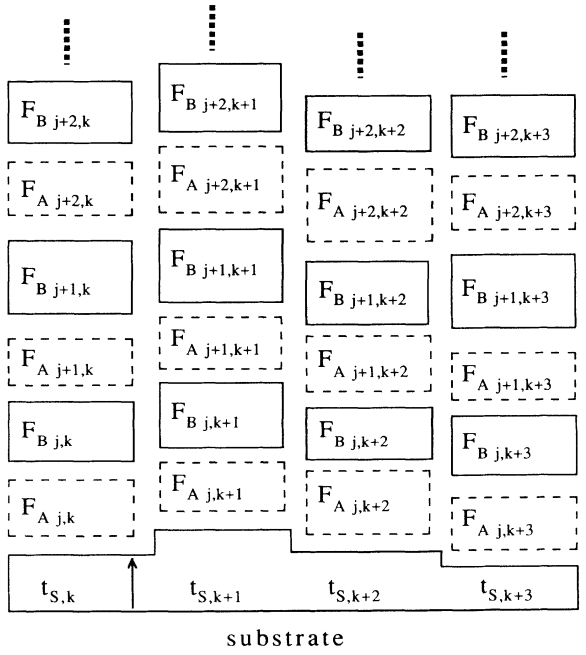

FIG. 4. Two-dimensional representation of a superlattice. Each column is described as in Fig. 1, and the additional substrate roughness is given by the offset $t_{S,k}$.

interface. This procedure is continued to the surface of the superlattice where the reflectivity R of the superlattice is calculated. The intensity of the reflected wave is then given by $I=|R|^2$.

Because optical theories do not include crystal structure of the layers in the calculations, but rather thickness and refractive index of the layers, layer thickness fluctuations are included by selecting randomly from the ensemble of possible layer thicknesses at each step in the recursion procedure. To determine the final intensity for the structural model shown in Fig. 2, the intensities of a large number of superlattices with difference, randomly selected thicknesses are calculated and averaged:

$$I=\frac{1}{N_{\rm av}}\sum_{n=1}^{N_{\rm av}}|R_n|^2 , \tag{17}$$

where R_n is the superlattice reflectivity for a superlattice with a particular random sequence of thicknesses and $N_{\rm av}$ is typically ≈ 100. The ensemble of thicknesses is determined by the structural parameters used in the high-angle calculations. In-plane averaging is accomplished by doing a finite average of R_n before the intensity is calculated for the model shown in Fig. 4. The intensity is given by

$$I=\frac{1}{N_{\rm av}}\sum_{n=1}^{N_{\rm av}}\left|\frac{1}{L}\sum_{l=1}^{L}R_{nl}\right|^2 , \tag{18}$$

where L is the number of random sequences that are averaged including the phase information.

In a number of systems, the interface is not chemically sharp but is interdiffused over a limited distance. A linear interdiffusion region was included in the low-angle calculations as described by Underwood and Barbee.[26] The interdiffusion region is calculated by a sequence of thin layers (≈ 0.1 Å) with an average index of refraction approximating the continuous change of the refraction index in the interdiffused region.

IV. MODEL

In a number of crystalline-crystalline superlattices, the average lattice constant $\bar{d}$ normal to the layers determined directly from the diffraction profiles has been found to vary as function of modulation. The model we use for a crystalline layer allows for deviations of the lattice constant near the interface as shown in Fig. 5. The crystalline layer is described by N atomic planes which are separated by a lattice constant d. Three atomic planes near the interface are allowed to expand or contract an amount $\Delta d_1 e^{-n\alpha}$ and $\Delta d_2 e^{-n\alpha}$, where $n=0,1,2$ corresponds to the first, second, and third atomic plane away from the interface. α is a constant that determines the decay of the strain away from the interface and is typically assumed to be 0.5. The structure factor for this layer is similar to Eq. (7) with the addition of the lattice deviation near the interface given by

$$F_j(q)=f(1+\exp[iq(d+\Delta d_1)]+\cdots+\exp\{iq[(N_j-1)d+(\Delta d_1+\Delta d_2)(1+e^{-\alpha}+e^{-2\alpha})]\}) . \tag{19}$$

Each layer is assumed to have an integer number of planes which varies about an average value $\bar{N}$. The average number of planes does not have to be restricted to an integer value. The distribution of the number of planes N_j for material A and B is given by a discrete distribution[49] about the mean values $\bar{N}_A$ and $\bar{N}_B$ with widths s_A and s_B. For large values of s, the distribution approximates a Gaussian distribution, and for small values the weighted average of the nearest integers. Because the width about a noninteger average is not an easily defined quantity, the values for s quoted in the paper is the standard deviation of the layer thickness resulting from discrete disorder. Equation (19) can be easily modified to include chemical interdiffusion by setting the scattering power of the atomic layers near the interface as a weighted average of material A and B.

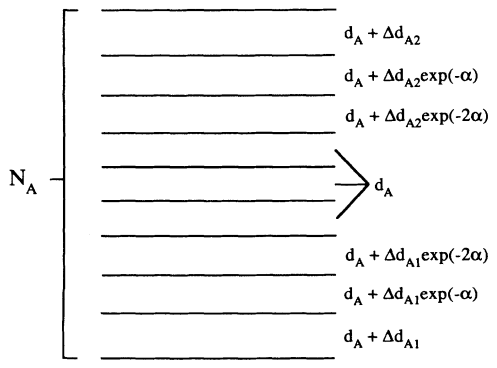

FIG. 5. Representation of a crystalline layer which is strained towards the interfaces. Lines represent atomic planes. Δd_1, Δd_2, and α determine lattice deviation near the interface.

The structure factor can be modified to include both the random fluctuations of the atomic lattice spacing and the intralayer strain profile [Eqs. (13) and (19)]. We have included the expressions for the averaged quantities including intra-layer disorder in the Appendix.

The parameters for the lattice expansion near the interface, Δd and α, were chosen to simulate a number of possible causes for lattice deviation near the interface. The possible mechanisms include chemical interdiffusion, coherency strains or dislocations, electron charge transfer across the interface, and surface relaxation resulting from an incoherent interface. The exact functional form of the lattice deviation near the interface is beyond the resolution of the x-ray-diffraction analysis. It is possible, however, to determine whether the measured deviation of the average lattice parameter is an interface property or continuous throughout the layer.

The scattering power of an atomic layer is given by

$$f(q)=\eta \exp[-\mathrm{DW}(q/4\pi)^2][f_0(q)+\Delta f'+i\Delta f''] , \quad (20)$$

where η is the in-plane atomic density and DW is the Debye-Waller coefficient, f_0 is the atomic scattering power which is strongly q dependent, and $\Delta f'$ and $\Delta f''$ are the anomalous dispersion corrections for the atomic scattering factor which are only weakly q dependent. The anomalous scattering parameters are generally small corrections, but can be quite large if the materials' absorption edge is near the x-ray wavelength used. The values of DW, $f_0(q)$, $\Delta f'$, and $\Delta f''$ are tabulated in International Crystallographic Tables.[50] The scattering power per unit volume ρ used in Eq. (11) is given by Eq. (20), replacing η by the atomic volume density. Chemical interdiffusion can be simulated by taking a weighted average of the scattering powers of the constituent materials.

V. FITTING PROCEDURE

To compare the measured x-ray-diffraction profiles of superlattices with the calculated profiles, additional corrections resulting from instrumental factors need to be included. The angle-dependent corrections of the intensity to a kinematical expression $I(q)$ include an absorption correction and the Lorentz-polarization factor. The final corrected intensity $I_c(q)$ to be compared with the measured profile is given by

$$I_c(q)=I(q)S\left[\frac{[1-\exp(-2\mu\tau/\sin\theta)](1+\cos^2 2\theta_m \cos^2 2\theta)}{\sin 2\theta}\right]+I_b , \quad (21)$$

where S is a scaling factor, μ is the average absorption coefficient, τ the total thickness of the superlattice, $2\theta_m$ the scattering angle of the monochromator, and I_b is the background intensity.

The peaks of the observed profiles are expected to be symmetrically broadened due to the limited instrumental resolution and asymmetrically broadened or split due to the $K\alpha_1$-$K\alpha_2$ doublet. The symmetrical broadening can be corrected by convoluting the calculated profiles with a Gaussian response function with a width corresponding to the resolution of the diffractometer ($\approx 0.08°$ in our case). The asymmetrical broadening can be taken into account by calculating the $K\alpha_1$ and $K\alpha_2$ contributions to the diffracted intensity separately and averaging the intensity values with the appropriate weighting factors (2:1). For most of the superlattices that we will discuss in this paper, the peaks were considerably broader than the instrumental resolution. In the cases where this is not true, both $K\alpha_1$-$K\alpha_2$ splitting and instrumental resolution were included in the model calculations.

To allow a quantitative comparison between the model calculations and the measured profiles, we have developed a nonlinear optimization program to refine the structure from the measured x-ray-diffraction profiles; the Superlattice Refinement from the x-ray-diffraction computer program (SUPREX).[51] The fitting procedure used was the Levenberg-Marquardt algorithm[52] where the structure parameters of the average unit cell including statistical fluctuations [Eq. (6)] are adjusted to minimize χ^2, the difference of the calculated and measured profiles squared. We would like to stress that in using this procedure, we are fitting the whole diffraction profile point by point, not simply relative intensities. No line-shape parameters are included; line shapes are determined by the structural parameters of the model. This is in contrast to the Rietveld technique where the relative peak intensities are determined by the scattering power of a single unit cell and the line shapes are fit to a structure independent profile shape function. Independent FORTRAN and TURBO-PASCAL versions were developed to crosscheck the accuracy of the results which were identical in both versions.

In most cases, only a subset of the possible fitting parameters are used. The fitting parameters used for a crystalline layer were the average number of atomic layers $\bar{N}$, the discrete fluctuation width s, the lattice spacing d, and the lattice deviation near the interface described by Δd_1, Δd_2, and α. The lattice spacing was allowed to fluctuate in a continuous Gaussian distribution of width δ about the average lattice spacing. Also fit was the interface distance a and the interface fluctuation width c. For an amorphous layer, the fitting parameters are the layer thickness t and the continuous layer fluctuation σ. The scale factor S and background intensity I_b in Eq. (21) were used as fitting parameters, although the background intensity was usually very close to zero. In most cases, some parameters were fixed in order to avoid overdetermining the problem. In particular, there is often a degeneracy in the interface distance a and the lattice expansions Δd_1 and Δd_2. To avoid this problem, the interface distance a was in many cases set equal to the average of the top atomic layer of layers A and B. The lattice expansions Δd_1 and Δd_2 were often set equal, although in some cases, an asymmetric strain profile ($\Delta d_1 \neq \Delta d_2$) was needed to obtain a good fit to the x-ray-diffraction profiles. The value of the exponent describing the lattice deviations near the interface α was usually fixed at a value of 0.5. In superlattices where the crystalline order of the layers is comparable, the values of δ_A and δ_B can be set to zero and only a continuous interface fluctuation c is used.

It is not uncommon for superlattice peaks to vary in intensity by four orders of magnitude. This large variation in intensity presents some difficulty in least-squares fitting since the larger peaks of the diffraction profiles will dominate the value of χ^2. In order to fit the whole profile we choose two alternatives for χ^2:

$$\chi^2=\sum_{i=1}^{N_{\mathrm{pnts}}}\left[\frac{I_c(i)-I_m(i)}{I_m(i)^{\epsilon}}\right]^2 , \quad (22)$$

$$\chi^2 = \sum_{i=1}^{N_{\text{pnts}}} \{\log_{10}[I_c(i)] - \log_{10}[I_m(i)]\}^2 , \quad (23)$$

where N_{pnts} is the number of points in the profile, I_c and I_m are the calculated and measured x-ray intensities, respectively, and ϵ an exponent defining the weighting factor of each point. The weighting factor is generally given by the uncertainty of the measured intensities, which in Poisson statistics is given by the square root of the number of counts, corresponding to $\epsilon = 0.5$. Typically, $\epsilon = 0.5$ was used in our fitting procedure, but if the lower intensity peaks were not reproduced, the value of ϵ was increased or the profile was fit on a log scale, given by the second definition of χ^2 in order to reduce the influence of the higher intensity peaks. All refinements presented in this paper used Eq. (22) with the appropriate choice of ϵ.

In general, we did not fit the low-angle profiles, but calculated them from the results of the high-angle fitting routine and compared the results. The low-angle profile is very sensitive to the alignment of the diffractometer. Moreover, the surface quality of the film and overlayers can greatly affect the results. In many cases, the rocking curve widths of the low-angle diffraction peaks are strongly q dependent which makes quantitative comparisons of the peak intensities very difficult. All these difficulties have a much smaller effect on the high-angle profiles. Since the low-angle profiles are not sensitive to the intralayer structure, they allow for checks of the interlayer parameters, layer thicknesses, and thickness disorder. There can be some difficulty in resolving discrete and continuous disorder in the high-angle profiles. It is particularly difficult to resolve the discrete disorder when the lattice spacing of the two constituent materials are closely lattice matched. The low-angle profiles are only sensitive to the size of the overall roughness independent of the nature of the roughness. Discrete disorder tends to be over a much longer length scale ($\approx 1-5$ Å) than the continuous disorder ($\approx 0.2-0.3$ Å), and will dominate the low-angle profiles. By qualitatively fitting the low-angle profiles, an estimate of the roughness can often be determined, which may set limits on the discrete disorder in the high angle.

Some care has to be taken when comparing the results of the high- and low-angle calculations. Low-angle scattering does not depend on the crystalline order within the layer which often results in the coherence length being much longer than in high-angle scattering. The longer coherence length combined with the low incident angle of the x rays may result in the low-angle scattering averaging over a much longer lateral distance in the layers than high-angle scattering. This problem of lateral averaging has been studied extensively for low-angle scattering from rough surfaces[53] and needs to be addressed for the case of superlattices.

VI. FITTING RESULTS

We will discuss the results of using the fitting algorithm on a number of different types of superlattice systems. These will include crystalline-crystalline systems made by sputtering, molecular beam epitaxy (MBE), and electroplating. To evaluate the reliability of the fitting method, we will concentrate on fitting results which can be compared directly with parameters determined independently by other methods. There are three types of structural parameters that are obtained from the refinement procedure: structural disorder, lattice constants, and chemical composition.

A. Layer thickness fluctuations

To determine the sensitivity of the x-ray structural refinement to cumulative layer thickness fluctuations, we have grown a series of Mo/Ni and Nb/Cu superlattices where layer thickness variations were introduced during the growth of the samples. The samples were made by dc magnetron sputtering onto ambient temperature sapphire and/or silicon substrates.[13] The substrates were rotated over the targets and held for predetermined amounts of time by a computer-controlled substrate holder in order to achieve the desired modulation wavelength. To introduce disorder into the layer thicknesses, the deposition time of the materials was varied randomly for each layer so that the layer thicknesses approximated a Gaussian distribution about the average layer thickness. Samples were made with thickness variations of only one of the constituent materials or with variations in both layers.

Previous work has shown that both Mo/Ni and Nb/Cu can be grown as high-quality superlattices.[13,47] The systems grow oriented with the Mo and Nb bcc(110) and the Ni and Cu fcc(111) planes perpendicular to the growth direction. X-ray scans were performed about the first-order [bcc(110)/fcc(111)] and second-order [bcc(220)/fcc(222)] portion of the profile. Examples of the diffraction profiles are shown in Fig. 6 for three $[\text{Mo}(20\text{ Å})/\text{Ni}(22\text{ Å})]_{130}$ superlattices, where the values in parentheses refers to the average layer thickness and the subscript gives the total number of bilayers. Figures 6(a) and 6(b) show the diffraction profiles of a sample without artificial roughness, Figs. 6(c) and 6(d) for a sample with 2.7 Å artificial roughness added to Ni, and Figs. 6(e) and 6(f) for a sample with 2.7 Å artificial roughness added to the Mo. The circles are the measured x-ray intensity and the solid line the structural refinement. The arrows indicate the expected peak positions for Mo and Ni. The effect of the additional disorder can be seen in both the relative intensity and linewidth of the profiles. As was predicted from earlier calculations,[38] increased disorder of the Mo (Ni) leads to broadening of the superlattice peaks associated with Ni (Mo). The second-order superlattice peaks are much more sensitive to discrete disorder. An artificial disorder of 2.7 Å is enough to almost completely suppress the second-order high-angle superlattice peaks.

The results of the structural refinement can be directly compared to the amount of additional artificial disorder introduced during growth. The samples without additional disorder have typical discrete disorder values of 1.0 Å, indicating the layers vary in thickness on average less than one monolayer. The value of the continuous disorder was 0.18 Å, which is in agreement with the values determined by Locquet *et al.*[37] and is close to the difference in the lattice spacing of Mo and Ni of 0.2 Å.

The amount of additional structural disorder, determined from the fits shown in Fig. 6 from the first- (second-) order peaks, is for Ni 2.0 (3.3) Å and for Mo 1.0 (2.6) Å, which is in good agreement with the values added during growth. There is a small discrepancy between the values determined from the first- and second-order portion of the profiles. The second-order values are in better agreement with the growth value. A possible explanation for the difference is that the second-order peaks are much more sensitive to discrete disorder and should give a more accurate measure of the disorder for a small amount of additional disorder. When the amount of disorder increases, this is no longer true. In samples with an additional 3.3 Å of roughness, the second-order superlattice peaks are no longer resolved. The refinement procedure can only give a lower limit of the disorder (≈ 3.5 Å). The first-order satellite peaks are still clearly resolved and give a more accurate measure of the roughness.

Shown in Fig. 7 are the parameters obtained from the structural refinement for all the Mo/Ni samples with artificial roughness. The amount of refined discrete roughness is plotted versus the amount of artificial roughness for three sets of Mo/Ni superlattices. The points correspond to samples with additional roughness added to the Mo or Ni layers individually or to both layers and

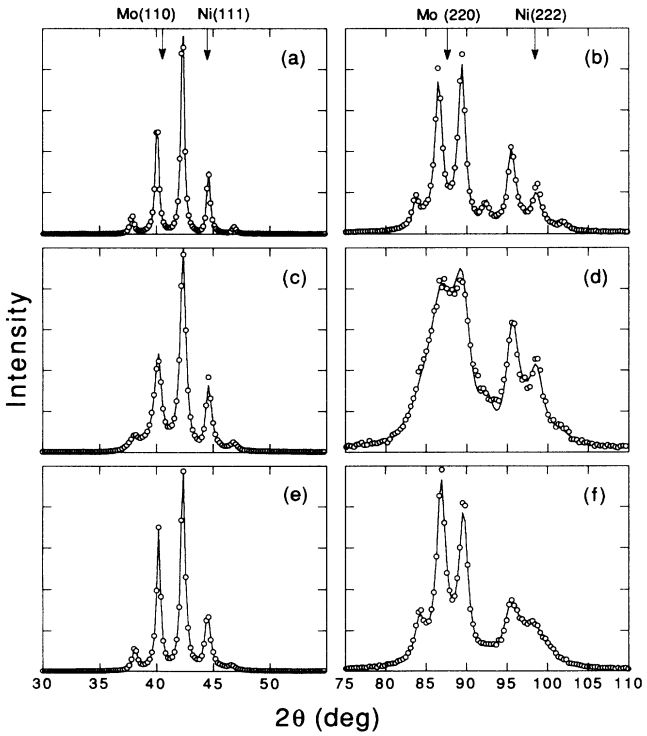

FIG. 6. Experimental profiles (○) and refined calculations (solid lines) of three [Mo(20 Å)/Ni(22 Å)]$_{130}$ superlattices: (a) and (b) without artificial roughness, (c) and (d) with 2.7-Å artificial roughness on the Ni layers, and (e) and (f) 2.7 Å on the Mo layers. The profiles on the left (a), (c), and (e) are taken around the first-order main Bragg reflections, the profiles on the right (b), (d), and (f) around the second order. All profiles are plotted on a linear scale and are normalized to the highest intensity.

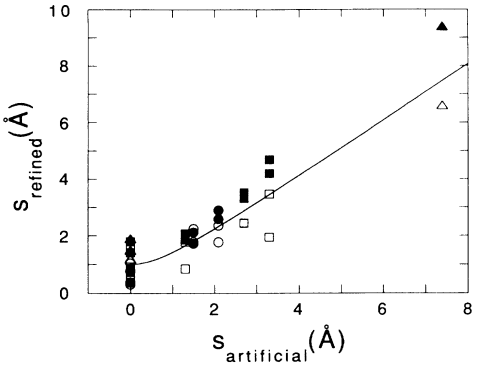

FIG. 7. The refined roughness vs artificial roughness for seven [Mo(13 Å)/Ni(16 Å)]$_{180}$ (circles), ten [Mo(20 Å)/Ni(22 Å)]$_{130}$ (squares), and four [Mo(27 Å)/Ni(33 Å)]$_{80}$ (triangles) superlattices. Open symbols are the roughness of Mo layers, the solid symbols of Ni layers. The line gives the expected behavior assuming 1.0-Å intrinsic roughness.

represent an average determined from averaging the first-order bcc(110)/fcc(111) and second-order bcc(220)/fcc(222) values. Solid and open symbols represent roughness values on Ni and Mo, respectively. The solid line is the expected relation between the refined roughness and artificial roughness assuming 1 Å of discrete roughness intrinsic to the layers,

$$S_{\text{refined}} = \sqrt{1\ \text{Å}^2 + S^2_{\text{artificial}}}\ .$$

In the refinement procedure, all the roughness parameters were fit, including interface disorder c and the intralayer disorder for both material δ_{Ni} and δ_{Mo}. Excellent quantitative agreement is obtained for all the samples which clearly shows that an additional amount of discrete disorder of less than a single lattice spacing can be quantitatively determined and resolved from the other disorder parameters.

Similar experiments were performed on a series of Nb/Cu superlattices. The difference in the Nb and Cu lattice spacing (0.25 Å) is larger than for Mo/Ni. Therefore, the diffraction profiles should be more sensitive to discrete disorder. X-ray-diffraction profiles from a series of [Nb(26 Å)/Cu(20 Å)]$_{40}$ is shown in Fig. 8 with no additional roughness (a) and (b) and 2.8 Å of additional roughness added to Cu (c) and (d) and Nb (e) and (f). The results of the discrete roughness as determined by x-ray refinement are given in Table I. In the sample with no additional disorder, the superlattice peaks about the Nb position are considerably broader than the peaks about the Cu position, indicating there is more discrete disorder in the Cu layers. (Note that this is contrary to what one may expect naively.) No superlattice peaks are observed about the Nb(220) peaks. The disorder values determined from the refinement about the first-order profile are continuous disorder of 0.3 Å and discrete disorder in the Nb (Cu) layers of 1.0 Å (3.7 Å). When additional artificial roughness is added to the Cu layers, the superlattice peaks around the Nb(110) reflection clearly broaden. The peaks about the Nb(220) are not clearly affected by the additional disorder on Cu. The Cu layers are already so

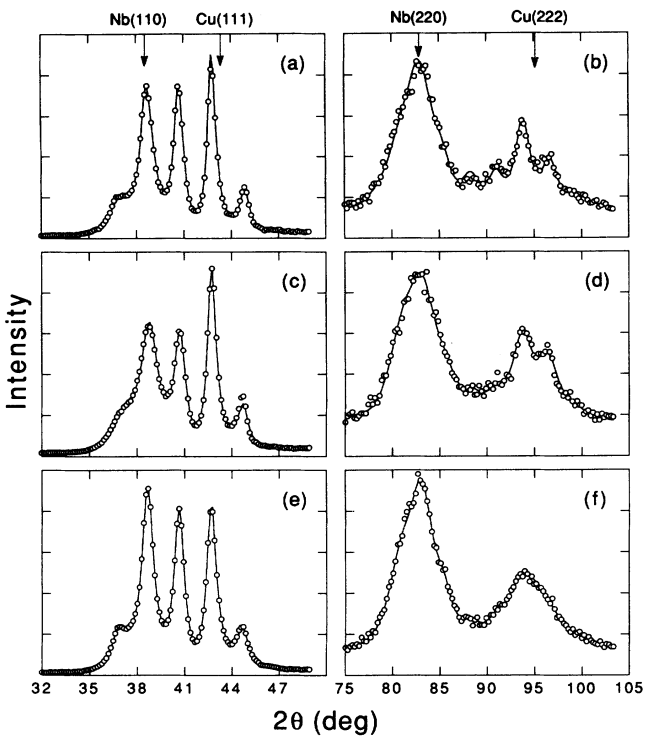

FIG. 8. Experimental profiles (○) and refined calculations (solid lines) of three [Nb(26 Å)/Cu(20 Å)]$_{40}$ superlattices: (a) and (b) without artificial roughness, (c) and (d) with 2.8-Å artificial roughness on the Cu layers, and (e) and (f) 2.8 Å on the Nb layers. The profiles on the left (a), (c), and (e) are taken around the first-order main Bragg reflections, the profiles on the right (b), (d), and (f) around the second order. All profiles are on a plotted on a linear scale and are normalized to the highest intensity.

rough that the superlattice peaks about the Nb(220) are not resolved and additional artificial roughness cannot be determined. Only a lower bound on the discrete roughness can be determined as shown in Table I. With additional roughness added to the Nb layer (c), the Nb and Cu layer roughness become comparable. This can lead to an uncertainty in the continuous and discrete disorder parameters during fitting because both terms now broaden the peaks and the limited number of higher-order satellite peaks limits the ability to resolve the different disorders. This leads to discrete disorder parameters that are slightly lower than expected for the first-order profile results and an increase in the continuous roughness parameters for this particular refinement.

The x-ray-diffraction profiles shown in Figs. 6 and 8 clearly demonstrate the need for including disorder parameters in a fitting model. The relative intensities of the peaks are strongly dependent on the amount of layer thickness fluctuations even though the lattice parameters and average layer thicknesses remain constant. This shows that relative intensity calculations to determine the lattice parameters without roughness included in the model may give anomalous results.

B. Lattice spacing

In many metallic superlattice systems, the average lattice spacing $\bar{d}$, which can be determined directly from the diffraction profiles, has been found to expand with decreasing Λ.[54] The expansion is thought to originate from strains introduced by the interfaces, but a quantitative understanding is lacking. Structural refinement of the x-ray-diffraction profile allows a determination of the individual lattice spacing of each of the constituent materials. Nb/Cu is an example of a system that shows an expansion of $\bar{d}$ with decreasing Λ. We have studied a series of sputtered Nb/Cu superlattices with equal Nb and Cu layer thicknesses, having a total thickness of 7 μm. The expansion of $\bar{d}$ relative to the bulk Nb and Cu values is determined by measuring a series of Nb/Cu superlattices as a function of Λ, keeping the relative concentrations constant and is given by the solid squares in Fig. 9(a).

The average lattice spacings of the Nb and Cu layers were determined by structural refinement of the reflection profiles. The parameters in the refinement were the continuous interface disorder c, average thickness of the layers $\bar{N}_{Nb}$ and $\bar{N}_{Cu}$, discrete disorder of the layers s_{Cu} and s_{Nb}, and the symmetric lattice expansion parameters Δd_{Nb} and Δd_{Cu}, with exponents set at $\alpha=0.5$. The bulk Nb and Cu lattice spacings were fixed at the measured values from sputtered Nb (2.346 Å) and Cu (2.087 Å) films. The interface distance was fixed at the average of the Nb and Cu lattice spacing closest to the interface. The best-fit values of the average Nb and Cu lattice spacings (the layer thickness divided by the number of atomic layers) are given in Fig. 9(b). The refinement gives the very interesting result that both layers are expanded relative to the bulk values, with the majority of the low Λ expansion confined to the Cu layer. The Cu discrete roughness is also strongly dependent on Λ. The discrete roughness for the $\Lambda=22$ Å and $\Lambda=30$ Å films was s_{Cu} and $s_{Nb}\approx 1$ Å. For the $\Lambda=55$ Å and $\Lambda=85$ Å films, there is an increase in s_{Cu} to 2.7 Å and >3.5 Å, respectively,

TABLE I. Refined roughness values compared to the artificial roughness for a series of Nb/Cu superlattices.

$S_{artificial}$ (Å)	$S_{refined}$ (Å)	
	Nb(110)/Cu(111)	Nb(220)/Cu(222)
$S_{Nb}=0.0$, $S_{Cu}=0.0$	$S_{Nb}=1.0$, $S_{Cu}=3.7$	$S_{Nb}=1.0$, $S_{Cu}>3.0$
$S_{Nb}=0.0$, $S_{Cu}=1.9$	$S_{Nb}=1.0$, $S_{Cu}=4.7$	$S_{Nb}=1.3$, $S_{Cu}>3.0$
$S_{Nb}=0.0$, $S_{Cu}=2.8$	$S_{Nb}=1.0$, $S_{Cu}=5.1$	$S_{Nb}=1.0$, $S_{Cu}>3.0$
$S_{Nb}=2.8$, $S_{Cu}=0.0$	$S_{Nb}=1.0$, $S_{Cu}=3.2$	$S_{Nb}=2.6$, $S_{Cu}>3.0$
$S_{Nb}=3.8$, $S_{Cu}=0.0$	$S_{Nb}=2.7$, $S_{Cu}=3.2$	$S_{Nb}>3.0$, $S_{Cu}>3.0$

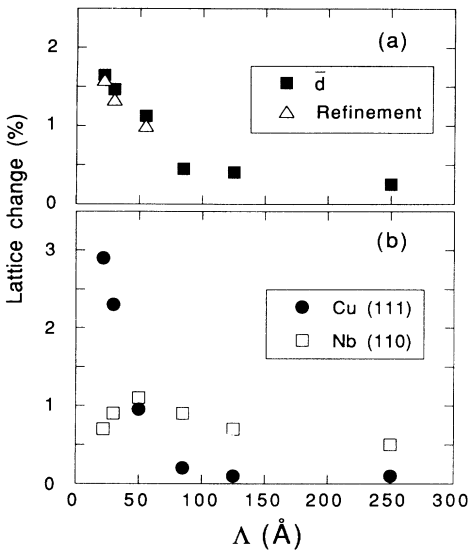

FIG. 9. (a) Expansion of the average lattice spacing $\bar{d}$ relative to the bulk value measured directly from the x-ray profiles (solid square) and determined from x-ray refinement (open triangles) and (b) the lattice expansion for Cu and Nb relative to bulk values obtained by structural refinement.

without a comparable increase in s_{Nb}. The increased Cu roughness was in agreement with the results shown in Fig. 8. To make a direct comparison, the expansion of $\bar{d}$ can be calculated from the best fit results of $\bar{N}_{Nb}$, $\bar{N}_{Cu}$, and the bulk lattice parameters of Nb and Cu and is shown in Fig. 9(a) as open triangles. Excellent agreement is found between the measured and refined expansion of $\bar{d}$.

Other techniques such as reflection high-energy electron diffraction (RHEED), extended x-ray-absorption fine structure (EXAFS), and x-ray photoelectron diffraction (XPD) can be applied to determine the local atomic distances in materials. A number of these techniques have been applied to a series of MBE grown Ag/Mn superlattices by Jonker *et al.*[55] RHEED studies found the Mn to initially grow lattice matched on the Ag and XPD (Ref. 55) and EXAFS (Ref. 56) were used to estimate the Mn lattice spacing in the growth definition. We have fit the measured x-ray-diffraction profiles to determine the Mn lattice spacing in the growth direction. These values are compared with the XPD and EXAFS results on the same superlattice samples, and XPD results on Ag/Mn/Ag trilayers.[57]

Figures 10(a) and 10(b) show the measured (circles) and fitted (line) diffraction profiles of 3- and 5-monolayer (ML) Mn superlattices, $[Ag(33\ Å)/Mn(6\ Å)]_{100}$ and $[Ag(31\ Å)/Mn(8\ Å)]_{20}$, respectively, about the Ag(002) peak. The fitting parameters used were $\bar{N}_{Ag}$, d_{Ag}, Δd_{Ag} with the exponent α set at 0.5, d_{Mn}, s_{Ag}, s_{Mn}, and continuous interface fluctuations c. An additional modified Lorentzian line shape[58] arising from the initial thick Ag buffer layer was also added into the fitting procedure, and the position is labeled by arrows on the plots. The diffraction profile is dominated by the Ag layers which are phase shifted relative to each other by the presence of the Mn layers. This makes a unique determination of the interface distance and Mn lattice spacing by the refinement very difficult for very thin Mn layers because the phase shift of Ag layers is given by $(N_{Mn}-1)d_{Mn}+2a$. Setting the interface to the average of $(d_{Ag}+\Delta d_{Ag}+d_{Mn})/2$ in the fitting allowed for a unique determination of the Mn distance.

Best-fit results for the Mn and Ag distances from fitting the diffraction profiles about the Ag[002] and Ag[004] reflections are given in Table II. Included in Table II are the Mn lattice spacings estimated from the c/a ratio determined from EXAFS and XPD on the same superlattices and XPD results on MBE grown Ag/Mn/Ag trilayers.[57] Excellent agreement is obtained between the three techniques for the Mn distance in the superlattices and for the lattice spacing in the trilayers.

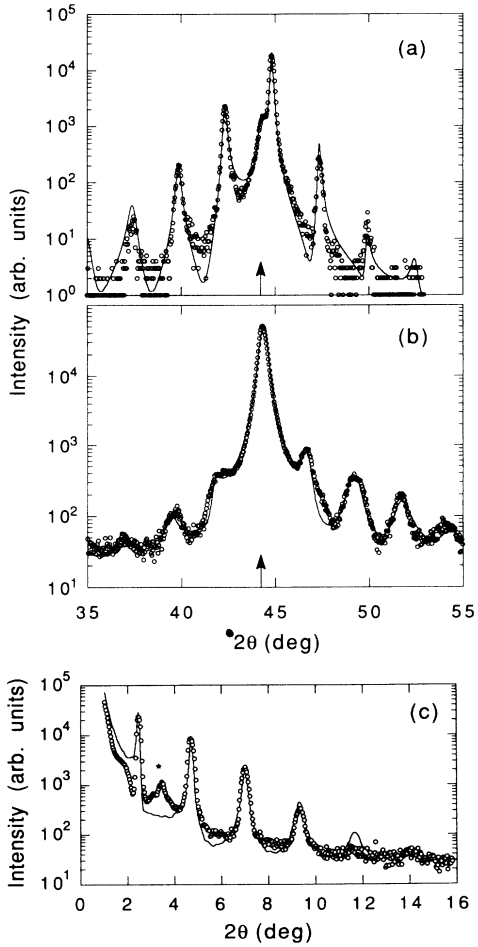

FIG. 10. Experimental (○) and calculated (solid line) high-angle x-ray-diffraction profiles for (a) $[Ag(33\ Å)/Mn(6\ Å)]_{101}$ and (b) $[Ag(31\ Å)/Mn(8\ Å)]_{20}$ superlattices. The refined parameters are given in Table II. The calculated spectra include $K\alpha_1$-$K\alpha_2$ splitting and instrumental line broadening of 0.05° 2θ. The arrows indicate the position of the addition Ag(002) buffer layer peak. (c) Experimental (○) and calculated (solid line) low-angle x-ray-diffraction profile for the $[Ag(33\ Å)/Mn(6\ Å)]_{60}$ superlattice using the refined parameters determined from the high-angle profile in (a). * indicate the peak resulting from capping layers.

TABLE II. Refined roughness and lattice parameters for MBE grown Ag/Mg superlattices. XPD results are obtained from Ref. 55 and EXAFS results are obtained from Ref. 56 where the Mn lattice spacings are estimated from the c/a ratio determined on the same superlattices. XPD results obtained from Ref. 57 (labeled XPD*) are for comparable Mn layer thicknesses in Ag/Mn/Ag trilayers.

Thickness (ML)		Roughness (Å)			Lattice spacings (Å)				
					X-ray		EXAFS	XPD	XPD*
N_{Ag}	N_{Mn}	S_{Ag}	S_{Mn}	c	d_{Ag}	d_{Mn}	d_{Mn}	d_{Mn}	d_{Mn}
15	5	2	1	0.23	2.046±0.003	1.68±0.04	1.64±0.08	1.66	1.65
16	3	1	1	0.08	2.051±0.003	1.90±0.04	2.03±0.15	1.91	1.80
13	2	2	0.5	0.04	2.052±0.003	1.92±0.04		1.91	1.85

In particular, all three techniques determines that there is a large change in lattice spacing from 3 to 5 ML of Mn. In the samples with 2 and 3 ML of Mn, the continuous roughness parameter c is very small, indicating that the interfaces have a high crystalline order. For the 5 ML of Mn sample, an increase in the continuous disorder parameter commensurate with the decrease of the Mn distance is observed. It is in qualitative agreement with the EXAFS measurements, which also determined increased disorder. The effect of the continuous disorder on the line width of the 5-ML sample can clearly be seen compared to the 3-ML profile and is indicative of a decrease in the crystalline order. The continuous disorder parameter in the 5 ML of Mn sample is comparable with values determined for lattice mismatched systems such as Mo/Ni,[37] and is comparable to the difference of the Ag and Mn lattice spacings.

Shown in Fig. 10(c) are the measured and calculated low-angle profiles for the same sample as shown in Fig. 10(a). The low-angle profile is calculated using the optical formalisms given in Eq. (17) and structural parameters determined from the fit shown in Fig. 10(a). The only adjusted parameters were the constant height and background. The peak labeled by the * results from capping layers. There is excellent quantitative agreement for the relative peak heights and widths. The results indicate that even layers with thicknesses as small as 3 ML can be well represented as continuous media with constant electron densities and, more important, the high-angle refinement parameters, in particular the discrete roughness, can reproduce the low-angle profile.

C. Chemical composition

In principle, the relative composition of the superlattice should be known from the growth conditions and be used as an input parameter for the refinement. However, problems in calibration and control of deposition often make accurate knowledge of the thicknesses difficult. Therefore, the thicknesses of the layers often needs to be included as fitting parameters. A number of techniques can be used to determine the chemical composition of the films directly and the results can be compared with the refinement values.

Shown in Fig. 11 is the x-ray-diffraction profile about the (200) reflections of a Cu/Ni superlattice prepared by electrochemical deposition.[59] The results for the relative composition from the x-ray refinement were Cu(23 Å)/Ni(28 Å) and $d_{Cu}=1.83$ Å slightly expanded compared to bulk (1.81 Å) and $d_{Ni}=1.75$ Å slightly contracted compared to bulk (1.76 Å). Chemical analysis of the films found a relative composition Cu(24 Å)/Ni(27 Å).[60] The results obtained with the refinement procedure are in excellent quantitative agreement considering that Cu and Ni are close in both lattice constant and scattering power which makes refinement of relative composition very difficult.

A series of W/Ni superlattices were sputtered under similar conditions where only the Ni sputtering rate, calibrated using a quartz crystal oscillator, was varied over a limited range and the W sputtering rate was kept fixed. X-ray refinement was applied to the diffraction profiles of all the samples. An example is shown in Fig. 12(a) for a $[W(26\text{ Å})/Ni(26\text{ Å})]_{20}$ superlattice, and the results for the relative W and Ni thicknesses are plotted versus the measured Ni sputtering rate in Fig. 12(b). The solid lines represent the expected thickness dependence on Ni sputtering rate. The uncertainty in the quartz crystal oscillator reading is ±0.2 Å/sec which corresponds to uncertainties in relative thicknesses of ±1 Å. The error bars on the points represent differences in the refined thicknesses depending on the fitting parameters used. The results are in very good agreement with the growth parameters with the W thickness remaining constant and Ni thickness increasing with Ni sputtering rate. Low-angle profiles indicated that a Ni rate of ≈6.0 Å/sec gave samples that were closest to equal layer thickness, which is in good agreement with the refinement.

It is often possible to obtain accurate measurements of

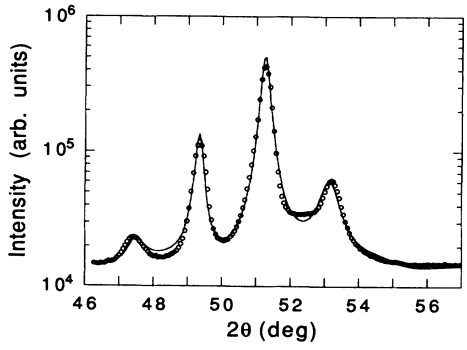

FIG. 11. Experimental (○) and calculated (solid line) x-ray-diffraction profile of a Cu(23 Å)/Ni(28 Å) superlattice about the (002) reflection.

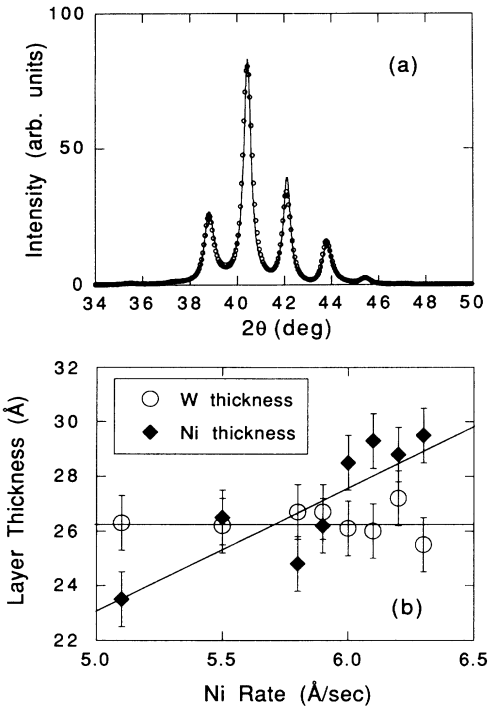

FIG. 12. (a) Experimental (○) and calculated (solid line) x-ray-diffraction profile of a $[W(26\ Å)/Ni(26\ Å)]_{20}$ superlattice. (b) Layer thicknesses of W and Ni obtained by structural refinement of a series of superlattices as a function of Ni sputtering rate.

the relative thicknesses from the low-angle profiles. When the layers have exactly equal thicknesses, the even-order low-angle peaks will be suppressed. When the thicknesses of the layers are not exactly equal, the shape of the even-order peaks will be dependent on the relative thicknesses of the layers. The interference of the reflected waves from the sample and the surface reflection can lead to dips in the diffraction profile near the Bragg angle.[12] This interference is most pronounced when the intensity of the Bragg scattering is very small and comparable with the surface reflections. The position of the dip relative to the Bragg angle is sensitive to which layer is thicker.[12,61,62] An example is given in Fig. 13. Figure 1 shows the refinement of a high-angle Mo/Ni profile which determined the thicknesses to be Mo(20 Å)/Ni(22 Å). Figure 13 shows the calculated low-angle diffraction profile for a Mo(22 Å)/Ni(20 Å) superlattice (curve 1), a Mo(20 Å)/Ni(22 Å) superlattice (curve 2), and the measured low-angle profile (curve 3) for the same sample shown in Fig. 1. The measured low-angle profile exhibits a well-resolved second-order peak, indicating that the layer thicknesses are not equal, and a dip at a slightly higher angle than the second-order Bragg peak. The position of the dip is in agreement with curve 2 which clearly demonstrates that the Ni layers are thicker than the Mo layers in agreement with the high-angle refinement results.

VII. DISCUSSION

The excellent agreement between the structural refinement calculations of superlattices and the values of

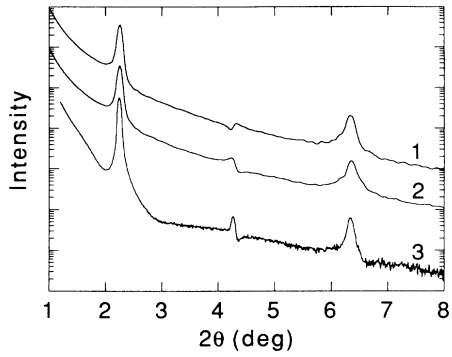

FIG. 13. The low-angle profiles are calculations for a Mo(20 Å)/Ni(22 Å) (curve 1) and a Mo(22 Å)/Ni(20 Å) (curve 2) superlattice, compared to the experimental profile (curve 3) of the same superlattice as in Fig. 1. Curve 2 was calculated for the parameters determined from the high-angle refinement shown in Fig. 1. The profiles have been offset for clarity.

independent measurements shows that quantitative results can be obtained for disorder, lattice spacing, and relative compositions. With careful analysis, these quantities can be determined with high accuracy.

A. Cautionary notes

Due to the number of parameters involved in a refinement and the complexity of relation (7), the multidimensional χ^2 surface becomes rather complex. Therefore, knowledge of the influence of the parameters on the diffraction profile and χ^2 is recommended. In complicated least-squares-fitting routines, it often happens that local minima prevent the algorithm from converging to the absolute minimum. Some care is needed in choosing starting parameters to avoid local minima. Erroneous parameters may be obtained if the model does not realistically describe the system that is fitted. If the model does not include the relevant parameters that describe the basic physics of the problem, other parameters may accommodate to account for the lacking parameters. For instance, if there is chemical interdiffusion at the interface which is not explicitly included in the fitting model, then lattice (deformation) expansions and contraction parameters will adjust to fit the changes in lattice spacing as a result of Vegard's law. Also, only random disorder is modeled, nonrandom correlated roughness is not included. This type of disorder only occurs in a limited number of systems, and has a different effect on the diffraction profiles as that predicted by the model presented here.[29]

χ^2 might also be insensitive to some parameters in a particular region of the parameter space or some parameters might be interdependent for a particular system. For example, the width of the continuous layer roughness of the amorphous Ge layers in a Pb/Ge superlattice has no effect on the high-angle profile once it becomes larger than 1.4 Å. Beyond this value the superlattice peaks disappear[11] and the continuous roughness should not be used as a fitting parameter. Therefore, the parameters that are optimized and eventually the sequence in which they are optimized should be selected with some care,

and reasonable starting parameters should be chosen. The most reliable fits are obtained by limiting the parameters that are fit to the ones most relevant to the problem.

The effects of discrete and continuous disorder has a qualitatively different effect on the diffraction profile. Discrete disorder leads to increased broadening of the lines with increasing order [n in Eq. (2)] of the diffraction peak away from the main Bragg, whereas continuous disorder leads to broaden all the peaks equally. If the highest-order peaks in the calculated profile (which tend to have the smallest effect on χ^2) are too broad, compared to the measured profile, the discrete roughness may need to be fixed at a smaller value so that the higher-order peak intensity and width are reproduced. This is usually only necessary for systems where the higher-order superlattice peaks are considerably weaker than the main Bragg peak.

It is essential that the parameters obtained during the fitting routine are checked for internal consistency. In the case of Nb/Cu and Mo/Ni, the average lattice spacing, $\bar{d}$, increases as the modulation length decreases indicating an expansion of the lattice spacing in the unit cell. The refined lattice spacings of the constituent materials should, on average, be consistent with this behavior (Fig. 8), although the fitting routine might also increase the relative contribution of the component with the larger lattice spacing to give an effective increased $\bar{d}$. The simulated diffraction profiles about the different main Bragg reflections should be consistent with one another. Resolved superlattice peaks about the second-order Bragg reflections, for example, can set an upper limit to the roughness, as we have discussed for Nb/Cu and Mo/Ni (Figs. 5–7 and Table I), or the low-angle profile can give an indication about the relative thicknesses (Fig. 13). The relative thicknesses should also be consistent with the growth conditions.

It can be very helpful to refine a series of samples where one of the parameters is changed systematically like Λ or the thickness of one of the layers. This can help to determine whether disorder is truly localized at the interface, implied by the continuous disorder interface parameter c, or is intrinsic to the layers. If there is an intralayer disorder δ for a layer which has N atomic planes, the continuous fluctuation of the total layer thickness will be $\sqrt{N}\,\delta$. If the refined value of c scales with the square root of the number of atomic planes, this may indicate an intralayer disorder and not strictly an interface effect. An estimate of δ may also be obtained from fitting the width of the Bragg peak of a thin film of each constituent material.

B. Application to other superlattice and thin films

The structural refinement procedure has been applied to several other superlattice systems. The crystalline-amorphous Pb/Ge system does not have high-angle superlattice peaks due to continuous thickness fluctuations of the amorphous Ge.[11] Only a finite-size-limited diffraction peak of the decoupled Pb layers can be seen, modified by discrete disorder.[63] With continuous random intralayer disorder in the Pb layer, the high-angle profile can be precisely reproduced by the refinement procedure.[64]

High-quality Y-Ba-Cu-O/Gd-Ba-Cu-O high-temperature superlattices have been synthesized by sputtering,[65] and the x-ray-diffraction profiles show sharp superlattice peaks. By specifying the structure factors, including metal ion and oxygen planes in the unit cell and chemical interdiffusion of the rare-earth sites, for both layers in Eq. (6), Eq. (7) is immediately available to refine these structures. It is found that a discrete disorder of one unit cell and limited interdiffusion can quantitatively fit the widths and relative intensities of Bragg and superlattice reflections. The same formalism can be used to refine the spectra of thin films, where the same material is designated for material A and B and different types of disorder such as stacking faults can be included in the averages.

VIII. CONCLUSION

We have shown that structural refinement of x-ray-diffraction profiles from superlattices can provide quantitative information about the lattice spacing and structural disorder of superlattice structures. A general kinematical one-dimensional diffraction formula, which includes random continuous and discrete fluctuations from the average structure and for which only the structure factor of one single layer of each material has to be averaged, is combined with a nonlinear fitting algorithm to fit the *entire* x-ray-diffraction profile, i.e., peak positions, relative intensities, and the line profiles. The results of the structural refinement were compared to results obtained independently from other measurements. To check the roughness values obtained by the refinement procedure, a series of Mo/Ni and Nb/Cu superlattices were prepared in which the layer thicknesses were varied during growth in a known random fashion. These values were very well reproduced by the refinement. Internal consistency was obtained by checking values obtained from various orders of reflections and from model-independent average quantities. Excellent agreement is obtained between the refinement results for the lattice parameters of Ag/Mn,

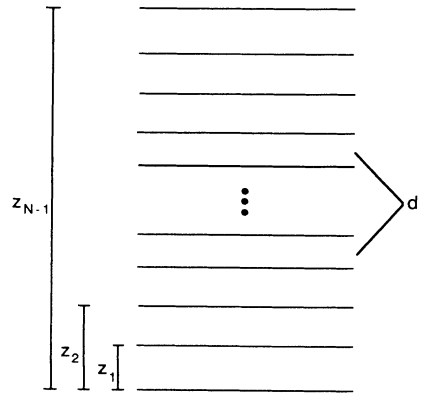

FIG. 14. Representation of a crystalline layer which is strained towards each interface. Lines represent atomic planes. The atomic planes three monolayers from the interface are allowed to deviate from the bulk lattice spacing d. All distances are referenced to the first atomic plane.

as compared to EXAFS and XPD. The relative thickness of the layers was accurately determined, and compared with chemical analysis for Cu/Ni, calibrated sputtering rate for W/Ni, and low-angle profile for Mo/Ni.

ACKNOWLEDGMENTS

We thank B. T. Jonker, G. Prinz, R. Oberle, and R. Cammarata for allowing the use of their x-ray data and S. Sinha, R. Dynes, J. Jorgensen, M. Grimsditch, D. McWhan, B. Clemens, C. Falco, and G. Felcher for helpful discussion. This work was supported by DOE Grant No. DE-FG03-87ER45332 at UCSD and the Belgian Inter University Institute for Nuclear Science, the Inter University Attraction Poles and Concerted Action Programs at KUL. International travel support was provided by the Belgian National Science Foundation and NATO.

APPENDIX

In this appendix we present the quantities Φ, T, $\bar{F}$, and $\langle F^*F \rangle$ of Eq. (7) for a layer consisting of N atomic planes, where the jth plane has an average distance z_j with respect to the first plane as shown in Fig. 14. The three planes closest to the interface deviate with respect to the bulk interplanar spacing d, but we will not give a specific form of the lattice deviations near the interface. All the interplanar spacings may deviate from the average d by the amount ∂ with respect to the previous plane in a similar fashion as described in Eq. (13) where all lattice fluctuations are assumed to be cumulative. The ∂'s are assumed to have a continuous Gaussian distribution about zero with width δ.

The structure factor for this layer is given by

$$F=f\left\{1+\exp[iq(z_1+\partial_1)]+\exp[iq(z_2+\partial_1+\partial_2)]+\exp[iq(z_3+\partial_1+\partial_2+\partial_3)]F'\right.$$
$$\left.+\exp\left[iq\left[z_{N-3}+\sum_{k=1}^{N-3}\partial_k\right]\right]+\exp\left[iq\left[z_{N-2}+\sum_{k=1}^{N-2}\partial_k\right]\right]+\exp\left[iq\left[z_{N-1}+\sum_{k=1}^{N-1}\partial_k\right]\right]\right\}, \tag{A1}$$

where F' is the structure factor for a single crystalline layer:

$$F'=\sum_{j=0}^{N-7}\exp\left[iq\left[jd+\sum_{k=1}^{j}\delta_j\right]\right]. \tag{A2}$$

Here we average over the continuous variables ∂_j by integrating over all real values ∂_j weighted by a Gaussian distribution. The average quantity $\bar{F}$ is given by

$$\bar{F}=f\{1+\exp(iqz_1-\gamma)+\exp(iqz_2-2\gamma)+\exp(iqz_3-3\gamma)\bar{F}'$$
$$+\exp[iqz_{N-3}-(N-3)\gamma]+\exp[iqz_{N-2}-(N-2)\gamma]+\exp[iqz_{N-1}-(N-1)\gamma]\}, \tag{A3}$$

where $\gamma=q^2\delta^2/2$ and $\bar{F}'$ is given by

$$\bar{F}'=\frac{1-\exp[(N-6)(iqd-\gamma)]}{1-\exp(iqd-\gamma)}. \tag{A4}$$

The averaged quantity T is given by

$$T=\exp[iqz_{N-1}-(N-1)\gamma]. \tag{A5}$$

Φ is given by

$$\Phi=f^*\left\{\exp[iqz_{N-1}-(N-1)\gamma]+\exp[iq(z_{N-1}-z_1)-(N-2)\gamma]+\exp[iq(z_{N-1}-z_2)-(N-3)\gamma]\right.$$
$$\left.+\left\langle\exp\left[iq\left[z_{N-1}-z_3+\sum_{k=4}^{N-1}\partial_k\right]\right]F'^*\right\rangle+\exp[iq(z_{N-1}-z_{N-3})-2\gamma]+\exp[iq(z_{N-1}-z_{N-2})-\gamma]+1\right\}, \tag{A6}$$

where

$$\left\langle\exp\left[iq\left[z_{N-1}-z_3+\sum_{k=4}^{N-1}\partial_k\right]\right]F'^*\right\rangle=\exp[iq(z_{N-1}-z_3)]\frac{\exp[-(N-4)\gamma]-\exp[-iq(N-6)d-2\gamma]}{1-\exp(-iqd+\gamma)}. \tag{A7}$$

$\langle F^*F \rangle$ is given by

$$\langle FF^* \rangle=ff^*\sum_{k=1}^{7}\sum_{l=1}^{7}\langle k,l \rangle, \tag{A8}$$

where $\langle k,l \rangle$ is the average of the kth term in within the large parentheses of Eq. (A1) times the complex conjugate of the lth term within the large parentheses of Eq. (A1). The $\langle k,k \rangle$ equals 1 for $k \neq 4$ and $\langle 4,4 \rangle = \langle F'F'^* \rangle$. The $\langle k,l \rangle$ terms for $k \neq l$ are the complex conjugate of $\langle l,k \rangle$ so there sum gives 2 times the real part of the $\langle k,l \rangle$ term. The full expression of Eq. (A8) is quite lengthy, so we will give some example terms of Eq. (A8):

$$\langle 2,1 \rangle + \langle 1,2 \rangle = \langle \exp[iq(z_1+\partial_1)] + \exp[iq(z_1+\partial_1)] \rangle = 2\cos(qz_1)\exp(-\gamma) , \tag{A9}$$

$$\langle 4,4 \rangle = \langle F'F'^* \rangle = N-6+\sum_{j=1}^{N-7}(N-6-j)2\cos(qjd)\exp(-j\gamma) , \tag{A10}$$

$$\begin{aligned}\langle 4,1 \rangle + \langle 1,4 \rangle &= \langle \exp[iq(z_3+\partial_1+\partial_2+\partial_3)]F' + \exp[-iq(z_3+\partial_1+\partial_2+\partial_3)]F'^* \rangle \\ &= 2\exp(-3\gamma)[\cos(qz_3)\mathrm{Re}(\bar{F}') - \sin(qz_3)\mathrm{Im}(\bar{F}')] ,\end{aligned} \tag{A11}$$

$$\begin{aligned}\langle 5,4 \rangle + \langle 4,5 \rangle &= \left\langle \exp\left[iq\left[z_{N-3}-z_3+\sum_{n=4}^{N-3}\partial_n\right]\right]F'^* + \exp\left[-iq\left[z_{N-3}-z_3+\sum_{n=4}^{N-3}\partial_n\right]\right]F' \right\rangle \\ &= 2\,\mathrm{Re}\left[\exp(z_{N-3}-z_3)\frac{\exp[-(N-6)\gamma]-\exp[-iq(N-6)d]}{1-\exp(-iqd+\gamma)}\right] ,\end{aligned} \tag{A12}$$

and $\langle 7,4 \rangle + \langle 4,7 \rangle$ is given by twice the real component of Eq. (A7).

Equations (A1)–(A12) are derived for a single integer number of atomic planes N averaged over cumulative variations of the lattice positions. To further average over discrete layer thickness fluctuation, the quantities Φ, T, $\bar{F}$, and $\langle F^*F \rangle$ must be calculated for various values of N and averaged, weighted by the probability of occurrence of each N. Equations (A1)–(A12) were derived for $M \geq 7$. Explicit analytical expressions for all integer values of $M < 7$ have to be derived in a way analogous to the equations outlined above.

[1]For recent reviews, see various articles in, for instance, *Physics, Fabrication and Applications of Multilayered Structures,* edited by P. Dhez and C. Weisbuch (Plenum, New York, 1988); in *Metallic Superlattices, Artificially Structured Materials,* edited by T. Shinjo and T. Takada (Elsevier, Amsterdam, 1987); in *Synthetically Modulated Structures,* edited by L. L. Chang and B. C. Giessen (Academic, New York, 1985); I. K. Schuller, J. Guimpel, and Y. Bruynseraede, Mater. Res. Bull. **XV**, 29 (1990).

[2]E. Spiller, in *Physics, Fabrication and Applications of Multilayered Structures,* edited by P. Dhez and C. Weisbuch (Plenum, New York, 1988), p. 271.

[3]F. Mezei, in *Physics, Fabrication and Applications of Multilayered Structures,* (Ref. 2), p. 310.

[4]J. Murduck, D. W. Capone II, I. K. Schuller, S. Foner, and J. B. Ketterson, Appl. Phys. Lett. **52**, 504 (1988).

[5]M. N. Baibich, J. M. Broto, A. Fert, F. Nguyen Van Dau, F. Petroff, P. Etienne, G. Creuzet, A. Friederich, and J. Chazelas, Phys. Rev. Lett. **61**, 2472 (1988).

[6]S. Hashimoto and Y. Ochiai, J. Magn. Magn. Mater. **88**, 211 (1990).

[7]H. M. Rietveld, J. Appl. Cryst. **2**, 65 (1969).

[8]F. Izumi, in *Advances in The Rietveld Method,* edited by R. A. Young (Oxford University Press, Oxford, in press).

[9]B. D. Cullity, *Elements of X-Ray Diffraction* (Addison-Wesley, London, 1978), p. 102.

[10]P. F. Miceli, D. A. Neumann, and H. Zabel, Appl. Phys. Lett. **48**, 24 (1986).

[11]W. Sevenhans, M. Gijs, Y. Bruynseraede, H. Homma, and I. K. Schuller, Phys. Rev. B **34**, 5955 (1986).

[12]D. Neerinck, K. Temst, H. Vanderstraeten, C. Van Haesendonck, Y. Bruynseraede, A. Gilabert, and I. K. Schuller, Mater. Res. Soc. Symp. Proc. **160**, 599 (1990).

[13]I. K. Schuller, Phys. Rev. Lett. **44**, 1597 (1980).

[14]V. S. Speriosu and T. Vreeland, Jr., J. Appl. Phys. **56**, 1591 (1984).

[15]J. M. Vandenberg, D. Gershoni, R. A. Hamm, M. B. Panish, and H. Temkin, J. Appl. Phys. **66**, 3637 (1989).

[16]J. M. Vandenberg, M. B. Panish, H. Temkin, and R. A. Hamm, Appl. Phys. Lett. **53**, 1920 (1988).

[17]J. C. P. Chang, T. P. Chin, K. L. Kavanagh, and C. W. Tu, Appl. Phys. Lett. **58**, 1530 (1991).

[18]A. Segmüller and A. E. Blakeslee, J. Appl. Cryst. **6**, 19 (1973).

[19]D. B. McWhan, in *Synthetic Modulated Structures,* edited by L. L. Chang and B. C. Giessen (Academic, Orlando, 1985), p. 43.

[20]D. B. McWhan, M. Gurvitch, J. M. Rowell, and L. R. Walker, J. Appl. Phys. **54**, 3886 (1983).

[21]J. Mattson, R. Bhadra, J. B. Ketterson, M. B. Brodsky, and M. Grimsditch, J. Appl. Phys. **67**, 2873 (1990).

[22]M. B. Stearns, C. H. Lee, and T. L. Groy, Phys. Rev. B **40**, 8256 (1989).

[23]G. Gladyszewski, Thin Solid Films **170**, 99 (1989).

[24]G. Gladyszewski and P. Mikolajczak, Appl. Phys. A **48**, 521 (1989).

[25]T. Shinjo, N. Nakayama, I, Moritani, and Y. Endoh, J. Phys. Soc. Jpn. **55**, 2512 (1986).

[26]J. H. Underwood and T. W. Barbee, Appl. Opt. **20**, 3027 (1981).

[27]P. Lee, Appl. Opt. **22**, 1241 (1983).

[28]R. W. James, *The Optical Principles of Diffraction of X-Rays* (Cornell University Press, New York, 1965).

[29]I. K. Schuller, M. Grimsditch, F. Chambers, G. Devane, H. Vanderstraeten, D. Neerinck, J.-P. Locquet, and Y. Bruynseraede, Phys. Rev. Lett. **65**, 1235 (1990).

[30]P. Auvrey, M. Baudet, and A. Regreny, J. Appl. Phys. **62**, 456 (1987).

[31]S. Hendricks and E. Teller, J. Chem. Phys. **10**, 147 (1942).

[32]J. Kakinoki and Y. Komura, J. Phys. Soc. Jpn. **7**, 30 (1952).

[33]M. Seul and D. C. Torney, Acta Crystallogr. Sect. A **45**, 381

(1989).

[34]For a general discussion of the effects of disorder on x-ray-diffraction profiles, see A. Guinier, *X-Ray Diffraction in Crystals, Imperfect Crystals, and Amorphous Materials* (Freeman, San Francisco, 1963), Chaps. 5–9.

[35]Y. Fujii, T. Ohnishi, T. Ishihara, Y. Yamada, K. Kawaguchi, N. Nakayama, and T. Shinjo, J. Phys. Soc. Jpn. **55**, 251 (1986).

[36]B. M. Clemens and J. G. Gay, Phys. Rev. B **35**, 9337 (1987).

[37]J.-P. Locquet, D. Neerinck, L. Stockman, Y. Bruynseraede, and I. K. Schuller, Phys. Rev. B **39**, 3572 (1988).

[38]J.-P. Locquet, D. Neerinck, L. Stockman, Y. Bruynseraede, and I. K. Schuller, Phys. Rev. B **39**, 13 338 (1989). We note that in Eq. (4) of this paper the number of interfaces in one of the terms was incorrect which leads to a minor correction.

[39]P. A. Kearney, J. M. Slaughter, K. D. Powers, and C. M. Falco, SPIE Proc. **984**, 24 (1988).

[40]For an overview see, T. W. Barbee, Jr., SPIE **563**, 2 (1985); Opt. Eng. **25**, 8 (1986).

[41]P. G. Harper, SPIE **984**, 150 (1988).

[42]B. Pardo, L. Nevot, and J.-M. Andre, SPIE **984**, 166 (1988).

[43]E. Spiller, and A. E. Rosenbluth, Opt. Eng. **25**, 954 (1986).

[44]H. Vanderstraten, D. Neerinck, K. Temst, Y. Bruynseraede, E. E. Fullerton, and I. K. Schuller, J. Appl. Cryst. **24**, 571 (1991).

[45]B. Vidal and P. Vincent, Appl. Opt. **23**, 1794 (1984).

[46]I. S. Gradzshteyn and I. M. Ryzhik, *Tables of Integrals, Series and Products* (Academic, New York, 1963), p. 494.

[47]M. R. Khan, C. S. L. Chun, G. P. Felcher, M. Grimsditch, A. Kueny, C. M. Falco, and I. K. Schuller, Phys. Rev. B **27**, 7186 (1983).

[48]M. Born and E. Wolf, *Principles of Optics* (Pergamon, Oxford, 1975), pp. 67–70.

[49]The discrete distribution about a noninteger average value $\bar{N}$ is calculated by taking Gaussian distributions centered about each of the nearest integer values with equal widths and the heights scaled by the difference of $\bar{N}$ and the integer values. For example, if $\bar{N}=14.3$, the Gaussians about 14 and 15 will have heights of 0.7 and 0.3, respectively. $P(N_j)$ values are then determined by taking the integrated intensity of the both Gaussian distributions ± 0.5 of N_j and normalizing to the total probability. This distribution for small widths gives just the weighted probability of the nearest integer values and for large widths approximates a Gaussian about $\bar{N}$.

[50]*International Tables for X-ray Crystallography IV* (Kynoch, Birmingham, 1974), p. 149.

[51]The SUPREX program is available for a number of different computers and in two different languages (FORTRAN and turboPASCAL) by writing to the authors (I.K.S. or Y.B.).

[52]P. R. Bevington, *Data Reduction and Error Analysis for the Physical Sciences* (McGraw-Hill, New York, 1969).

[53]S. K. Sinha, E. B. Sirota, S. Garoff, and H. B. Stanley, Phys. Rev. B **38**, 2297 (1988).

[54]I. K. Schuller and M. Grimsditch, J. Vac. Sci. Technol. B **4**, 1444 (1986).

[55]B. T. Jonker, J. J. Krebs, and G. A. Prinz, Phys. Rev. B **39**, 1399 (1989).

[56]Y. U. Idzerda, B. T. Jonker, W. T. Elam, and G. A. Prinz, J. Appl. Phys. **67**, 5385 (1989).

[57]W. F. Egelhoff, Jr., I. Jacob, J. M. Rudd, J. F. Cochran, and B. Heinrich, J. Vac. Sci. Technol. A **8**, 1582 (1990).

[58]The line shape used in the refinement was $y=H\{1+[(x-x_0)/\Gamma]^{\tau}\}^{-1}$, where H, x_0, Γ, and τ are the height, center, width, and exponent, respectively, that define the line shape and are used as fitting parameters. $\tau=2$ corresponds to a Lorentzian line shape.

[59]L. H. Bennett, L. J. Swartzendruber, D. S. Lashmore, R. Oberle, U. Atzmony, M. P. Dariel, and R. E. Watson, Phys. Rev. B **40**, 4633 (1989).

[60]R. Oberle (private communication).

[61]L. M. Goldman, H. A. Atwater, and F. Spaepen, Mater. Res. Soc. Symp. Proc. **160**, 578 (1990).

[62]The position of the dip can be qualitatively understood from simple phase arguments. There is a difference of a π rotation of the electric field upon reflection of the x rays from the more dense to less dense interface (Mo to Ni) compared to the less dense to more dense interface (Ni to Mo). When the layer thicknesses are equal, the even-order Bragg reflections are suppressed because the Ni-Mo reflections destructively interfere with the Mo-Ni reflections at even-order Bragg angles. When the layer thicknesses are not equal, the cancelation will not be complete at the even-order Bragg angles leading to a small even-order peak. The phase sign will depend on whether the denser material is thicker or thinner than the less dense material, so the interference between the surface reflection and Bragg reflection shifts will shift dependent on the relative thickness of the layers.

[63]D. Neerinck, H. Vanderstraeten, L. Stockman, J.-P. Locquet, Y. Bruynseraede, and I. K. Schuller, J. Phys.: Condens. Matter **2**, 4111 (1990).

[64]I. K. Schuller, E. E. Fullerton, H. Vanderstraeten, and Y. Bruynseraede, Mater. Res. Soc. Symp. Proc. **229**, 41 (1991).

[65]O. Nakamura, E. E. Fullerton, J. Guimpel, and I. K. Schuller, Physica C **185-189**, 2069 (1991).